Published March 1, 1988

The Sodium Current Underlying Action Potentials in Guinea Pig Hippocampal CA1 Neurons

P. SAH, A. J. GIBB, and P. W. GAGE

From the Department of Physiology, John Curtin School of Medical Research, Australian National University, Canberra 2601, Australia

ABSTRACT Neurons were acutely dissociated from the CA1 region of hippocampal slices from guinea pigs. Whole-cell recording techniques were used to record and control membrane potential. When the electrode contained KF, the average resting potential was about −40 mV and action potentials in cells at −80 mV (current-clamped) had an amplitude >100 mV. Cells were voltage-clamped at 22–24°C with electrodes containing CsF. Inward currents generated with depolarizing voltage pulses reversed close to the sodium equilibrium potential and could be completely blocked with tetrodotoxin (1 μM). The amplitude of these sodium currents was maximal at about −20 mV and the amplitude of the tail currents was linear with potential, which indicates that the channels were ohmic. The sodium conductance increased with depolarization in a range from −60 to 0 mV with an average half-maximum at about −40 mV. The decay of the currents was not exponential at potentials more positive than −20 mV. The time to peak and half-decay time of the currents varied with potential and temperature. Half of the channels were inactivated at a potential of −75 mV and inactivation was essentially complete at −40 to −30 mV. Recovery from inactivation was not exponential and the rate varied with potential. At lower temperatures, the amplitude of sodium currents decreased, their time course became longer, and half-maximal inactivation shifted to more negative potentials. In a small fraction of cells studied, sodium currents were much more rapid but the voltage dependence of activation and inactivation was very similar.

INTRODUCTION

Signal transmission in nervous systems depends on action potentials that are generated by voltage-dependent conductances. In squid axon and other peripheral nerves, membrane depolarization activates a voltage-dependent sodium conductance and it is generally thought that a sodium conductance with similar properties underlies action potentials in neurons in the mammalian central nervous system. This assumption has been difficult to test experimentally, both because it is difficult to insert two electrodes into mammalian central neurons in order to voltage-clamp the membrane and because it is not possible to control

Address reprint requests to Dr. P. W. Gage, Dept. of Physiology, John Curtin School of Medical Research, Australian National University, P.O. Box 334, Canberra 2601, Australia.

the membrane potential in axonic and dendritic processes of neurons with electrodes in the soma. A voltage-dependent sodium conductance has been characterized in cat motoneurons (Barrett and Crill, 1980), in rat nodose ganglion cells (Ikeda et al., 1986), and in cultured sympathetic ganglion neurons (Belluzzi and Sacchi, 1986), but not in cerebral neurons. We have used a single-electrode, switching voltage clamp (Brenneke and Lindermann, 1974; Finkel and Redman, 1985) to control membrane potential in CA1 neurons acutely dissociated (Numann and Wong, 1984) from guinea pig hippocampal slices. The dissociation procedure produced many cells consisting of a soma with few processes that generated large sodium currents in response to membrane depolarization. Preliminary accounts of some of these results have been published elsewhere (Sah et al., 1986).

METHODS

Hippocampal Slices

All experiments were performed with cells dissociated from the hippocampus of 300–500-g male or female adult guinea pigs. Animals were killed by cervical dislocation and the brain was quickly exposed. The brain was hemisected and dissected in cold (4–8°C) Krebs solution of the following composition (millimolar): 125 NaCl, 5.0 KCl, 25 $NaHCO_3$, 2 $MgSO_4$, 2.5 $CaCl_2$, 1.2 NaH_2PO_4, 11 glucose, pH 7.3 when bubbled with 95% O_2/5% CO_2. The hemisected brain was then glued to the stage of a Vibraslice (model 752, Campden Instruments) with cyanoacrylic glue. Sections 600 μm thick were then taken through the cerebral cortex and hippocampus to produce transverse hippocampal slices, which were transferred to a dish of cold, oxygenated Krebs. The CA1 region in each slice was isolated using fine iridectomy scissors. This piece of tissue was then cut into two or three smaller pieces, each ~1.5 mm square. Dissociation was performed with a protocol very similar to that described by Numann and Wong (1984).

Dissociated Cells

Papain (24 U/ml) and cysteine (5 mM) (Sigma Chemical Co., St. Louis, MO) were dissolved in 15 ml of oxygenated Krebs. Pieces of hippocampus were placed in this solution at room temperature and rapidly stirred. After ~90 min, the pieces were taken out of the papain solution with a Pasteur pipette and transferred to a holding beaker containing Krebs solution. Individual pieces of tissue were removed and mechanically dissociated as needed by trituration with a fire-polished Pasteur pipette in 3–4 ml of solution. The dispersed cells and debris were decanted into 5-cm plastic petri dishes where, after 5–10 min, the cells settled to the bottom. The petri dishes were mounted on the stage of an inverted phase-contrast microscope (Olympus IM) and viewed at a magnification of 400. Cell viability was aided by blowing a stream of moistened 95% O_2/5% CO_2 over the surface of the dish. Although the yield of cells was extremely variable, 10–20 healthy cells could be obtained, on average, from each piece of tissue.

Electrodes

Patch recording electrodes were made from hematocrit tubes (borosilicate glass) on a modified electrode puller (David Kopf Instruments, Inc., Tujunga, CA) and coated with Sylgard (Dow Corning Corp., Midland, MI) to within 100 μm of the tip to reduce electrode capacitance. Electrodes were held in an electrode holder with a side arm allowing

suction to be applied to the electrode interior. The electrode holder was plugged directly into the ×1 headstage of an Axon 2A (Axon Instruments, Inc., Burlingame, CA) single-electrode voltage-clamp device.

Electrodes were filled with a solution containing (millimolar): 140 CsF, 10 NaCl, 10 HEPES-CsOH, 11 EGTA, pH 7.2. In some experiments, the CsF was replaced with KF and the pH was balanced with HEPES-KOH. These electrodes had resistances of 1–3 MΩ. High intracellular fluoride, as noted elsewhere (Fernandez et al., 1984; Kay and Wong, 1986), greatly aided recording stability.

Voltage Clamp

Under visual control, the electrode tip was pressed against the surface of the cell and gentle suction was applied to the electrode interior to form an electrode–cell membrane seal of several gigohms' resistance (Hamill et al., 1981). Further suction and hyperpolarization of the patch resulted in membrane breakdown, giving low-resistance access to the interior of the cell.

With a switched current or voltage clamp, series resistance is not a source of error, but it was found necessary to keep the electrode resistance low in order to achieve the rapid switching rate and high clamp gain necessary to clamp the sodium currents adequately. Typically, recordings were made with switching rates between 20 and 40 kHz and a gain setting of 20–50 nA/mV. The headstage of the clamp was continuously monitored to ensure that the voltage across the electrode had settled completely before the membrane potential was sampled (Finkel and Redman, 1985). Under optimum conditions, with the clamp switching at 50 kHz and a gain of 50 nA/mV, the membrane voltage in response to a small voltage step reached 95% of the command voltage within 500 μs.

Data Analysis

Voltage-clamp commands and data sampling were performed on-line with a PDP 11/23 microcomputer (Digital Equipment Corp., Marlboro, MA). Voltage and current traces were filtered at 4 kHz (four-pole Bessel, −3 dB) and sampled at 10 or 20 kHz. In some experiments, data acquisition was performed with a digital oscilloscope (5211A, Tektronix, Inc., Beaverton, OR) at rates of up to 200 kHz and then transferred to the computer.

Currents were analyzed off-line on a PDP 11/44 computer (Digital Equipment Corp.) after subtraction of scaled leakage and capacitive currents obtained from hyperpolarizing steps (<50 mV). For each trace, the peak amplitude was measured from the peak inward current. The time to peak was measured from the onset of the voltage step.

Tetrodotoxin (TTX; Sankyo, Tokyo, Japan) and internal CsF were used to block sodium and potassium currents, respectively. In some experiments, the bath temperature was controlled with a Peltier element mounted on the microscope stage. The temperature of the dish was monitored by a small thermocouple placed in the bath solution. Most experiments were done at 22–24°C except where stated otherwise.

RESULTS

Cells obtained by dissociation displayed a wide variation in size and morphology. Healthy cells, recognized by their "shiny" appearance under phase-contrast optics (Numann and Wong, 1984; Gray and Johnston, 1985; Kay and Wong, 1986), normally retained some short (<100 μm) cell processes. The soma of most of the larger cells was bipolar, which suggests that they were probably pyr-

amidal cells (Kay and Wong, 1986). In this study, we have not discriminated between cells of different morphology but have tended to examine the larger cells, which turned out to have similar electrophysiological properties, except that a few (15 of 120) had faster sodium currents than the others. The type of sodium current more commonly seen will be described in detail, followed by a brief account of the "fast" sodium current.

Passive Electrical Properties

The average resting membrane potential, recorded from 28 cells with electrodes containing 150 mM KF, was -40 ± 2 mV (mean $\pm$ 1 SEM). This is more depolarized than expected for a membrane much more permeable to potassium than to other ions: with 5 mM K in the extracellular solution, the potassium equilibrium potential would have been -86 mV. The most likely explanation for the large difference between the recorded resting potential and the potassium equilibrium potential is that the stumps of fractured axons and dendrites formed a nonselective shunt across the surface membrane (see Discussion).

The input resistance of cells was determined either from the change in membrane potential produced by injection of rectangular current pulses or from the currents that flowed in response to steps in potential in voltage-clamped cells. The relationship between the clamp potential and current recorded in six cells (holding potential, -100 mV) can be seen in Fig. 1 *A*. The current-voltage curve was linear at membrane potentials between -120 and -80 mV and calculations of membrane resistance and capacity were therefore made from measurements in this potential range. The change in potential (upper trace) recorded in response to a hyperpolarizing current of 100 pA (lower trace) is shown in Fig. 1 *B*. A semilogarithmic plot of $V(\infty) - V(t)$ vs. time [$V(\infty)$ and $V(t)$ were the changes in potential at "infinite" time and time t, respectively] is shown in Fig. 1 *C*. It can be seen that the potential changed exponentially with a single time constant, which indicates that the cell was isopotential (Rall, 1977). With larger current pulses, the change in potential was no longer a single exponential, probably because of activation of the inward rectifier potassium channel (Adrian et al., 1970). The membrane time constant of a cell (τ_m) was obtained by fitting the potential change with a single exponential using a nonlinear least-squares algorithm. Time constants had values of 1.2–10 ms, with a mean of 5.0 ± 0.8 ($n = 16$). The input resistance (R_o), measured from $V(\infty)/I$ (I was the amplitude of the current pulse), ranged from 100 to 1,000 MΩ, depending on the size of the cell. Another method used to measure the passive electrical properties was to record currents generated by small hyperpolarizing or depolarizing voltage steps in a cell voltage-clamped at a holding potential of -100 mV. A typical current generated by a 30-mV depolarizing step (Fig. 1 *E*) is shown in Fig. 1 *D*. Values for R_o calculated from the slope of current-voltage relationships around -100 mV were similar to those obtained with the current-clamp method.

Input capacity (C_o) was calculated either from $\tau_m = R_o C_o$ or from the ratio of the integral of the capacity current to the amplitude of the voltage step. Values for C_o obtained in this way ranged from 5 to 50 pF, again depending on the size of the cell. The average value was 30.7 ± 5.8 pF ($n = 28$).

The specific membrane resistance and capacity were calculated by estimating the area of surface membrane: direct measurements were made of the cell length and diameter, and the surface area was calculated by assuming that the cell had a circular cross section along its long axis. The values for specific mem-

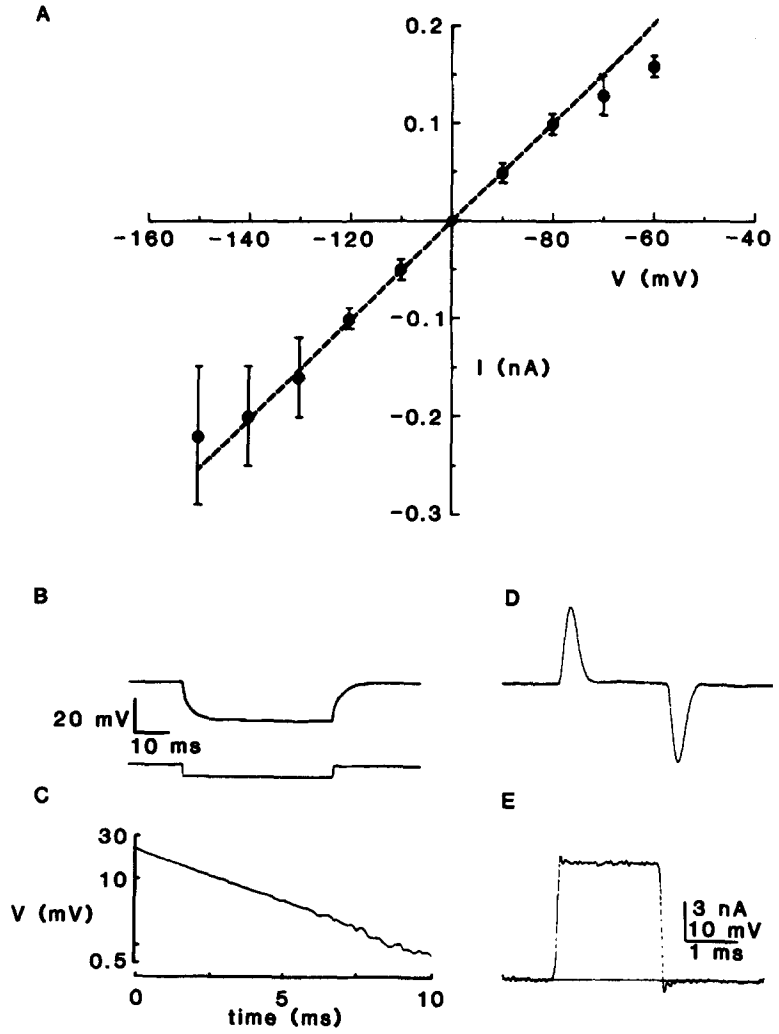

FIGURE 1. Passive membrane properties of dissociated hippocampal cells. (*A*) Current-voltage relationship. Currents were generated by voltage steps from −100 mV to the voltages shown on the abscissa. Data points are average values from six cells of a similar size. The broken line is the linear regression line of best fit for the points between −120 and −80 mV, which gave an input resistance of 200 MΩ. (*B*) Voltage response to a rectangular current of 100 pA. (*C*) Semilogarithmic plot of the decay of the voltage transient in *B*. (*D*) Current (filtered at 1 kHz) generated in a voltage-clamped neuron by a 30-mV depolarizing pulse (*E*) from a holding potential of −100 mV.

brane capacity ranged from 0.5 to 1.5 $\mu F \cdot cm^{-2}$, with a mean value of 1.0 ± 0.2 $\mu F \cdot cm^{-2}$ (n = 16). The specific membrane resistance ranged from 3.6 to 10.8 $k\Omega \cdot cm^2$, with a mean value of 5.8 ± 1.4 $k\Omega \cdot cm^2$ (n = 7).

Action Potentials

After establishment of recording conditions, spontaneous action potentials (Fig. 2 *A*), which could be blocked with TTX, were often seen. Long depolarizing currents produced trains of action potentials. In order to record action potentials at more negative potentials, cells were hyperpolarized to −80 mV by injecting

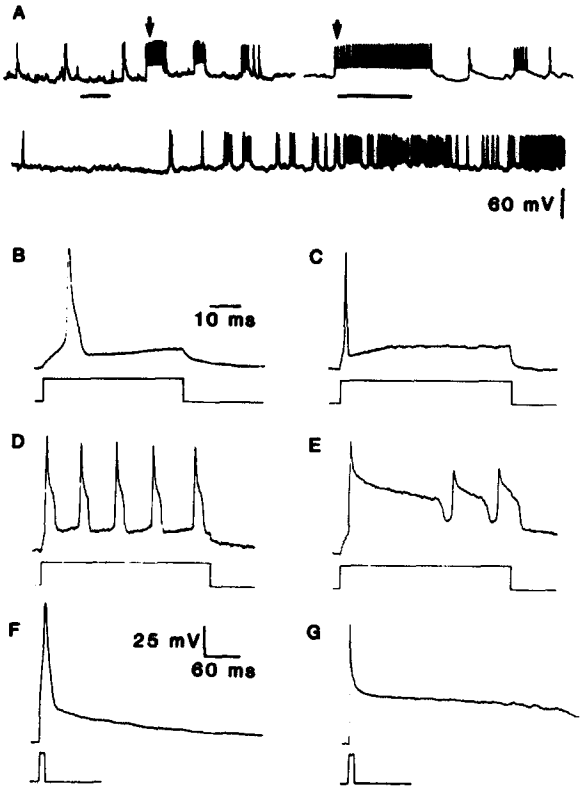

FIGURE 2. Action potentials recorded in cells perfused with KF. (*A*) Spontaneous action potentials recorded on a chart recorder. A depolarizing current (100 pA) was injected at the times marked by arrows. In the top trace, the time base has been expanded during the second segment: the horizontal scale bars represent 1 s. (*B–G*) Action potentials and trains of action potentials recorded from different cells in response to depolarizing currents shown in the lower trace of each record. Note that the time calibration for *B* is 10 ms, whereas the time calibration for *C–G* is 60 ms.

a maintained inward current. Action potentials were then elicited with brief (Fig. 2, *F* and *G*) or long (Fig. 2, *B–E*) depolarizing currents. Action potentials recorded in this way had an amplitude of ~100 mV (the average value from measurements in 15 cells was 103 ± 3 mV) and a rate of rise that ranged from 600 to 1,000 $V \cdot s^{-1}$. As can be seen in Fig. 2, *B–G*, the decay of action potentials was quite variable from cell to cell, ranging from 6 ms to hundreds of milliseconds. The longer action potentials were seen when the electrode contained CsF, presumably because potassium channels were blocked. In some cells, the membrane potential repeatedly "flipped" between two levels of potential. This phenomenon was not investigated further in this study.

Sodium Currents

Current-voltage relationship. In cells clamped with electrodes containing KF, currents evoked by depolarizing pulses from a holding potential of −100 mV consisted of a transient inward current followed by a sustained outward current (Fig. 3, *A* and *B*). The inward current disappeared in the presence of TTX (Fig. 3 *A*) and its amplitude was dependent upon the internal and external sodium concentrations (not shown). In many cases, a small inward current, assumed to be a calcium current, remained in the presence of TTX at concentrations as high

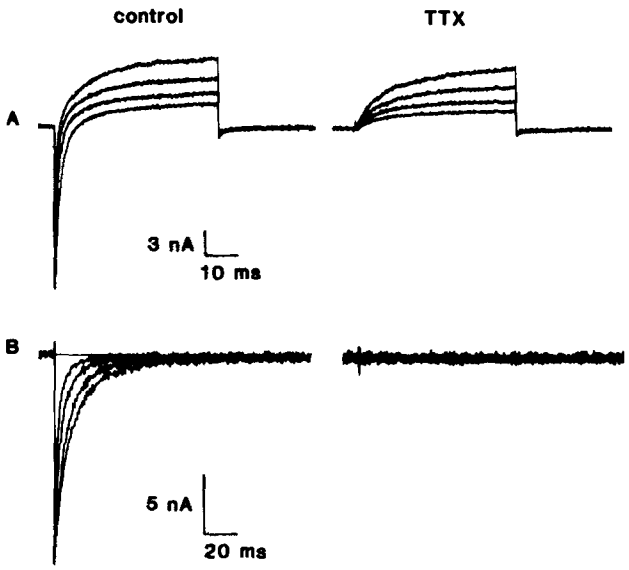

FIGURE 3. TTX blocks inward currents. The currents shown were generated by positive voltage pulses from a holding potential of −100 mV, before and after exposure to TTX (1 μM). (*A*) The perfusing solution was KF. Currents were generated by 50-ms voltage steps to −10, 0, 10, and 20 mV. TTX abolished the inward current, leaving only outward currents (right-hand panel). (*B*) When the perfusing solution was CsF, there was no outward current. Currents shown were generated by 100-ms voltage steps to −30, −20, −10, and 0 mV. In the presence of TTX, the inward currents disappeared (right-hand panel).

as 10^{-6} M (Fig. 5 *D*). It was concluded that the large, TTX-sensitive inward current was a sodium current and that it could be accurately described in the presence of the TTX-insensitive inward current because the latter was so much smaller (maximum amplitude, <0.5 nA; see also Kay et al., 1986). The outward current was not seen when the patch electrode contained CsF (Fig. 3 *B*) and its properties will be described elsewhere.

The properties of the TTX-sensitive sodium current were studied in cells clamped with electrodes containing CsF. A frequently observed phenomenon,

seen with small depolarizing steps from a holding potential of −100 mV, was the appearance of an inward current following a delay of 2–3 ms (Fig. 4 *A*). Often this phenomenon was associated with a voltage trace that revealed inadequate voltage control but, on occasion, the voltage did appear to be well con-

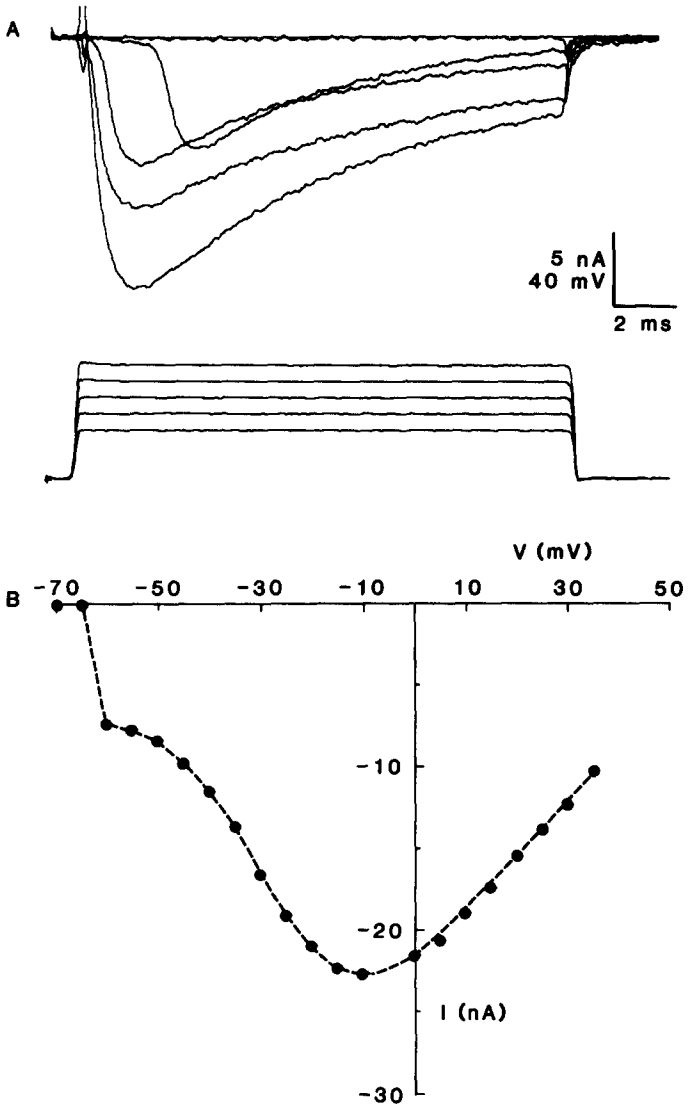

FIGURE 4. "Breakthrough" sodium currents (upper traces) generated by voltage steps (lower traces) to between −60 and −30 mV from a holding potential of −100 mV. (*B*) The peak current-voltage curve for the currents shown in *A* contains an obvious discontinuity at −60 mV.

trolled. These "breakthrough" currents produced a discontinuity in the current-voltage relationship (Fig. 4 *B*), as has been noted elsewhere (T. H. Brown et al., 1981; Barrett and Crill, 1980). Such currents were seen only in cells with long (>50 μm) processes and it was concluded that they were generated in remote, inadequately clamped patches of membrane, perhaps in the initial segment (Barrett and Crill, 1980) or dendrites. Cells that had these "breakthrough" currents were not used.

A typical family of sodium currents can be seen in Fig. 5 *A*. The relationship between peak current and membrane potential is plotted in Fig. 5 *C*. The amplitude was maximal at about −20 mV. The null potential for the current obtained by extrapolation was +58 mV. This is close to the calculated sodium equilibrium

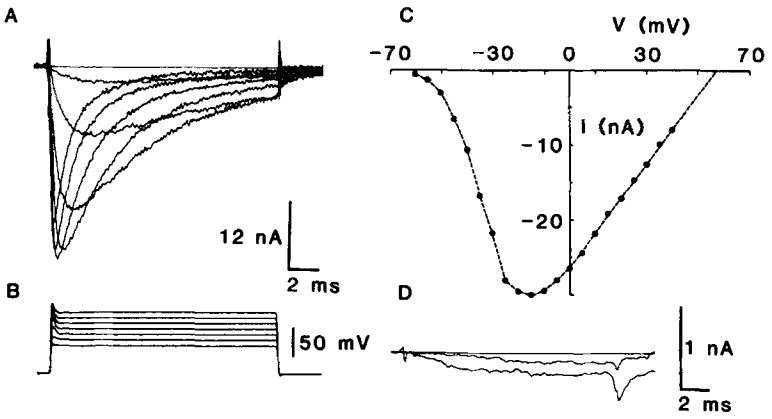

FIGURE 5. Inward currents recorded in voltage-clamped cells with an electrode containing CsF. (*A*) Sodium currents generated by potential steps from a holding potential of −100 mV to potentials between −50 and +10 mV (*B*: 10-mV increments). (*C*) Current-voltage curve from the same cell as in *A*. The extrapolated null potential was +58 mV. (*D*) Currents recorded in the presence of 1 μM TTX in response to voltage steps to −40 and −50 mV from a holding potential of −100 mV. These were the largest inward currents seen in the presence of TTX.

potential of +68 mV. The largest inward currents recorded in any cell in the presence of TTX (1 μM), presumed to be calcium currents (Kay et al., 1986), are shown in Fig. 5 *D* for comparison: they were relatively so small that no attempt was made to remove them. In most cells, TTX abolished all detectable inward current, as illustrated in Fig. 3.

It was possible to shift the null potential to less positive potentials by raising the sodium concentration in the electrode or by lowering the sodium concentration in the extracellular solution. Reversal of sodium current could then be obtained at membrane potentials where the kinetics of the current allowed the peak to be resolved. The peak current-voltage relationship obtained in a cell in an extracellular solution containing 50 mM NaCl (sodium replaced by choline)

can be seen in Fig. 6 (circles). The instantaneous current-voltage relationship measured from tail currents (Fig. 6, squares) was linear in the voltage range from −30 to 40 mV, which indicates that the sodium channel responsible for the current was ohmic (Hodgkin and Huxley, 1952*b*). At potentials more negative than −30 mV, the tail current decayed too rapidly for accurate measurement of its amplitude. The linear regression line (broken line) in Fig. 6 gave a null potential of +39 mV, close to the predicted equilibrium potential of +41 mV.

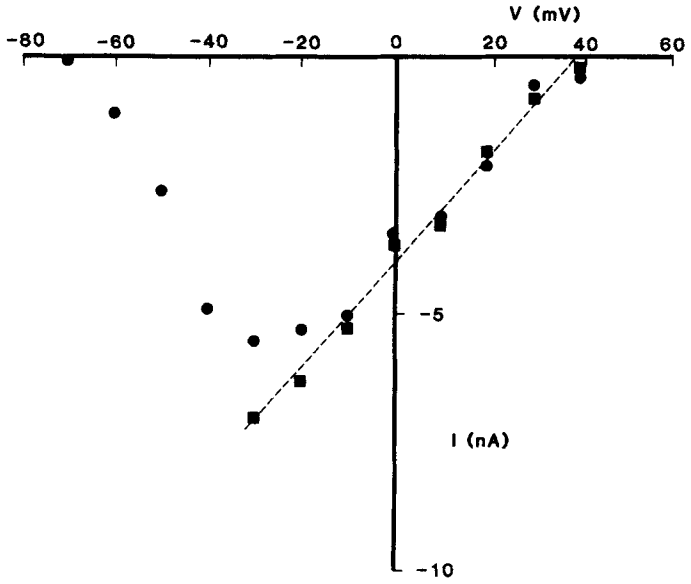

FIGURE 6. Current-voltage curve for the peak inward current (circles) in a dissociated neuron in an external solution containing 50 mM Na^+. The squares show the amplitudes of the instantaneous currents (holding potential, −100 mV). The null potential obtained from the linear regression line was +39 mV.

Conductance-voltage relationship. Because the instantaneous sodium current varied linearly with voltage (Fig. 6), the peak conductance was calculated from the equation (Hodgkin and Huxley, 1952*a*)

$$I_{Na} = g_{Na} \cdot (V - E_{Na}), \quad (1)$$

where I_{Na} is the peak current, g_{Na} is the conductance, E_{Na} is the measured sodium equilibrium potential, and V is the membrane potential. In cells in which an adequate instantaneous current-voltage relation could not be obtained, the equilibrium potential was obtained by extrapolation of the peak current-voltage relation. The typical relationship between potential and conductance at the peak of the current is shown in Fig. 7 *A*. The conductance increased sigmoidally with

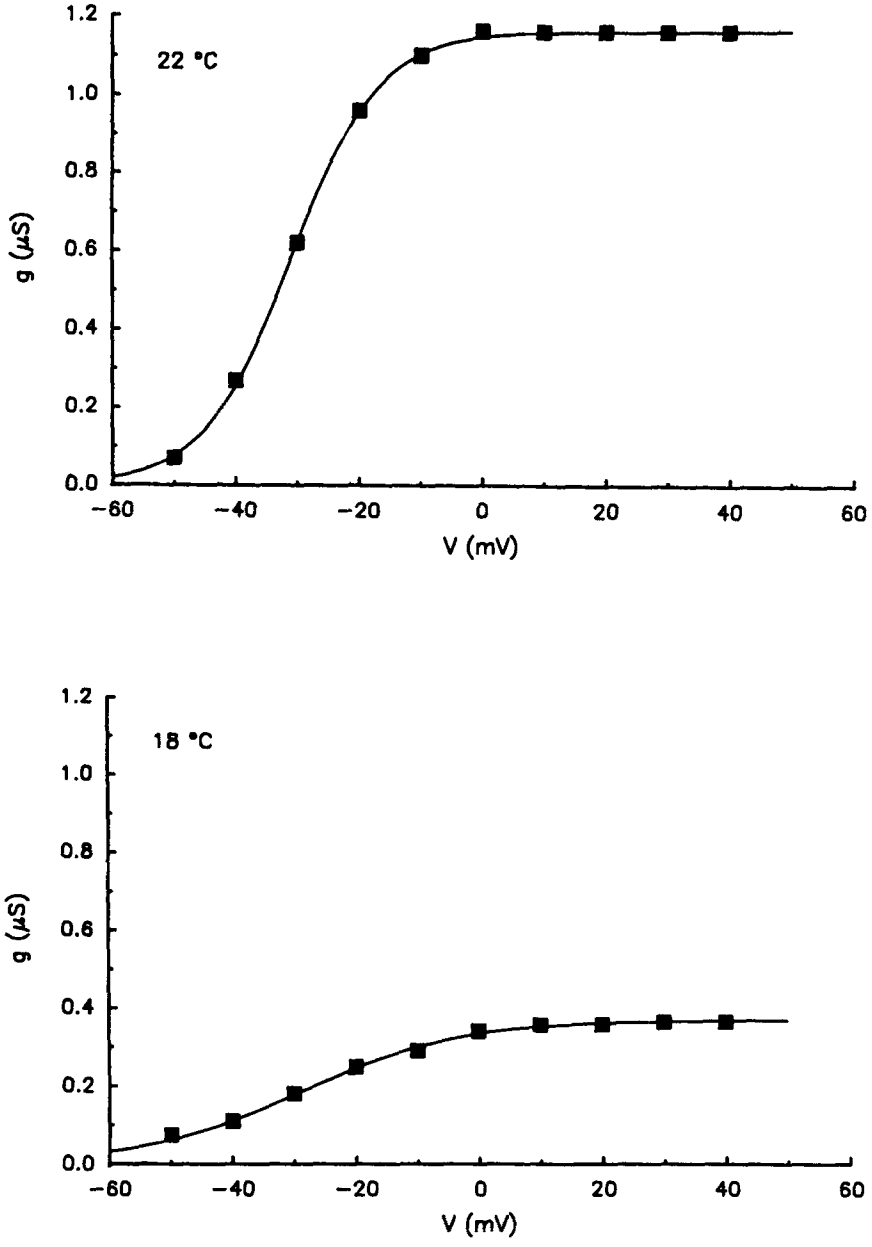

FIGURE 7. Peak sodium conductance (g) as a function of voltage (V). (A) The squares show conductance calculated according to Eq. 1 (E_{Na} = +65 mV) from the peak amplitude of currents recorded at 22°C. The solid line shows the best fit of Eq. 2 (see text). V' and k were −31 and 7.1 mV, respectively. (B) Conductance was calculated as in A from currents recorded at 18°C. V' and k values for the solid line were −29 and 13 mV, respectively.

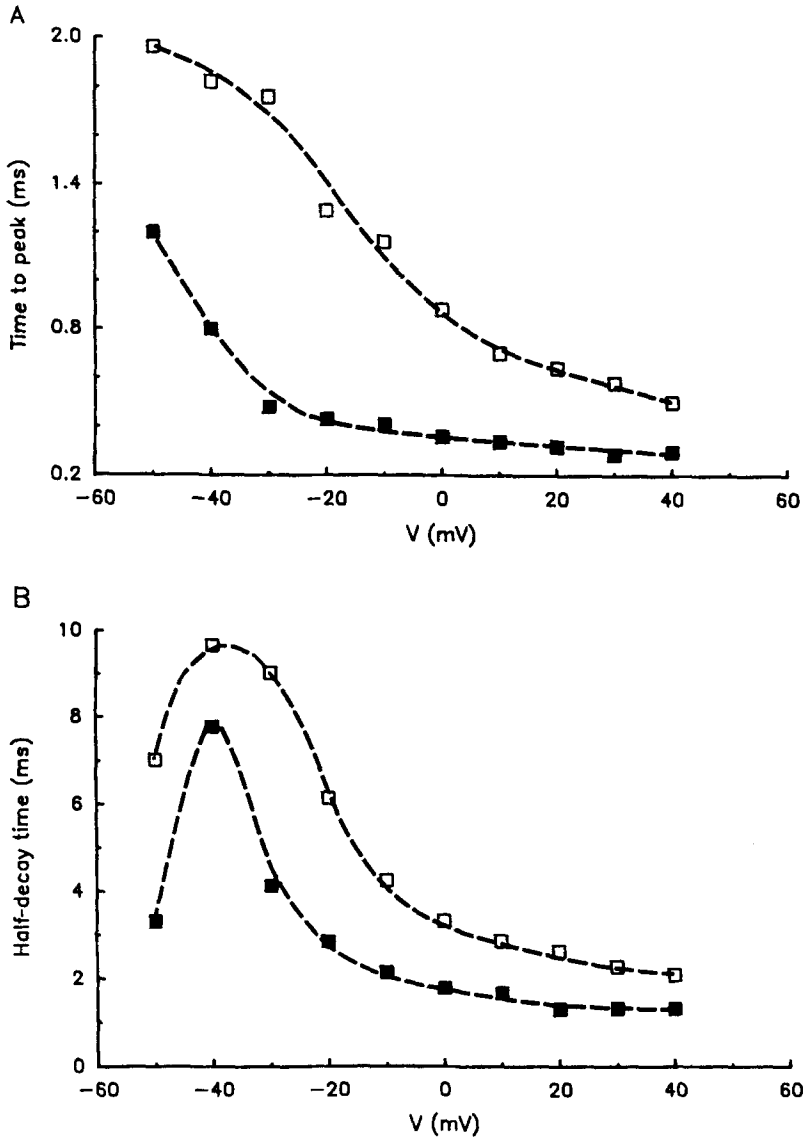

FIGURE 8. Time to peak (*A*) and half-decay times (*B*) (measured from the peak) of sodium currents recorded at different potentials in a cell at 22°C (filled squares) and at 18°C (open squares). Lines were drawn by eye.

potential at potentials more positive than −60 mV, reaching a maximum at about 0 mV. The line through the points in Fig. 7 *A* was obtained from the Boltzmann expression:

$$g_{Na} = g_{Na}(\max)/[1 + \exp(V' - V)/k], \quad (2)$$

where g_{Na}(max) is the maximum conductance, V' is the potential at which $g_{Na} = g_{Na}(max)/2$, and k is a slope constant: the values for V' and k used in Fig. 7 *A* were −31 and 7.1 mV. The average values for V' and k obtained in this way from eight cells were −38.7 ± 3.3 and 6.6 ± 0.3 mV, respectively.

No attempt was made to construct conductance-voltage curves by correcting for "inactivation" of channels, because the decay of the currents could not always be fitted with a single exponential (see below).

Time course of activation. It can be seen in Fig. 5 *A* that the rate of activation of the sodium current varied with membrane potential. A plot of the time to peak (measured from the onset of the voltage step to the peak of the current)

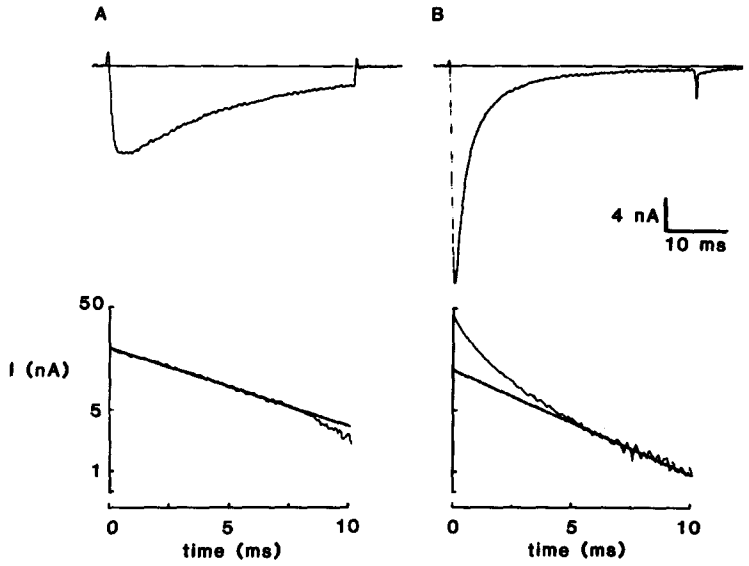

FIGURE 9. Decay of sodium currents generated by pulses to −40 mV (*A*) and to 0 mV (*B*) from a holding potential of −100 mV. The upper traces show the currents recorded and the graphs below contain semilogarithmic plots of their decays. The decay does not follow a single exponential at 0 mV.

against potential for a cell at 22°C is shown in Fig. 8 *A* (filled squares). The measurements at potentials more positive than −10 mV may contain some error since the potential was not fully controlled during the rising phase. An effort was made to overcome this problem by cooling the cell to 18°C. This slowed the time to peak (Fig. 8 *A*, open squares) so that measurements could be made with more confidence. It can be seen from Fig. 8 *A* that the rate of activation of sodium channels became progressively more rapid as the potential became more positive.

Time course of decay. The decay of currents could be reasonably described by a single exponential at potentials from −50 to −20 mV. A current elicited by a voltage step from a holding potential of −100 to −40 mV is shown in Fig. 9 *A* (upper trace). A semilog plot of the decay below could be well fitted with a

straight line. However, at potentials more positive than −20 mV, the decay could not be described by a single exponential, as illustrated in Fig. 9 *B*. The current in the upper panel was generated by a step to 0 mV from the same holding potential. A semilog plot of the decay of the current could no longer be fitted with a straight line (Fig. 9 *B*, bottom).

Because the decay of the currents could not always be described by a single exponential, the rate of decay of the current was characterized by the time to decay to half the maximum amplitude. A plot of half-decay time against membrane potential in a cell at 22°C is shown in Fig. 8 *B* (filled squares). The decay was slowest at about −40 mV and became faster at more positive potentials.

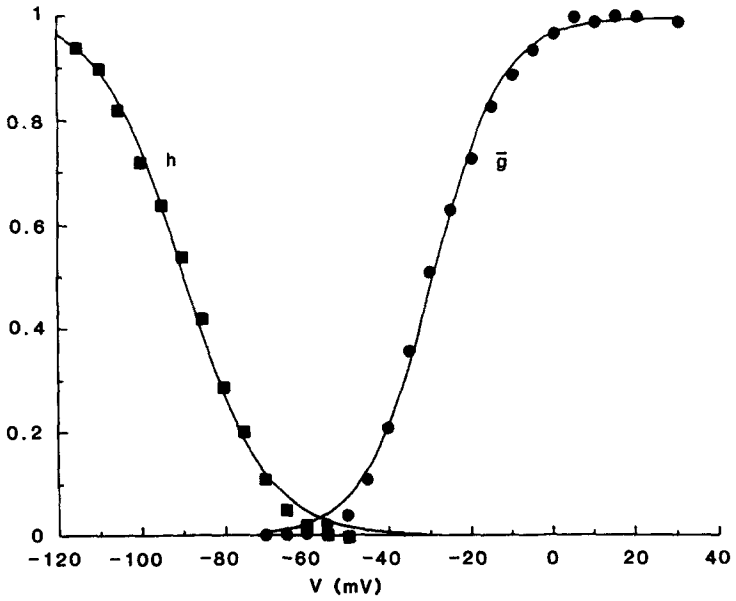

FIGURE 10. Steady state inactivation of sodium current. The amplitude of the sodium current generated by a pulse to −20 mV after a 1-s conditioning step to different potentials (abscissa) is expressed as a fraction (h) of the sodium current generated after a conditioning step to −120 mV (holding potential, −100 mV). The solid line through the data points is the line of best fit (Eq. 3) and gives a V' of −89.5 mV and a k of 9.9 mV. Normalized conductances ($\bar{g}$, circles), calculated from currents generated in the same cell by voltage steps to potentials shown on the abscissa from a holding potential of −100 mV, are shown for comparison.

Steady state inactivation. Steady state inactivation (h_∞) was studied by clamping a cell at a conditioning potential for 1 s before eliciting a sodium current with a 50-ms test pulse to −20 mV (holding potential, −100 mV). The amplitude of the sodium current measured at different conditioning potentials, expressed as a fraction (h_∞) of the amplitude when the conditioning potential was −120 mV, is plotted against the conditioning potential in Fig. 10 (squares).

The line through the points was drawn according to (Hodgkin and Huxley, 1952*b*)

$$h_\infty = 1/[1 + \exp(V - V')/k], \quad (3)$$

with a half-inactivation voltage (V') of −89.5 mV and a slope factor (k) of 9.9 mV. The normalized peak conductance in the same cell is plotted against potential for comparison (circles). The average values for V' and k recorded in eight cells were −74.9 ± 2.0 and 7.7 ± 1.0 mV, respectively.

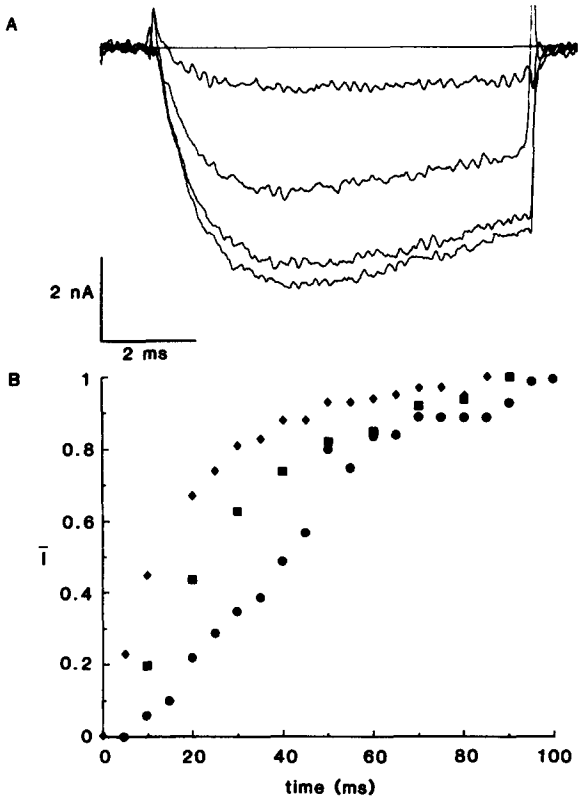

FIGURE 11. Recovery from inactivation. (*A*) Currents generated by a test pulse to −20 mV at 10, 30, 50, and 70 ms after a 100-ms conditioning pulse to 0 mV (holding potential, −100 mV). (*B*) Amplitude of sodium current after a conditioning depolarization, expressed as a fraction of the amplitude with no conditioning pulse ($\bar{I}$), plotted against time after a conditioning pulse. The graph shows data obtained with holding potentials of −80 (circles), −100 (squares), and −120 (diamonds) mV.

Recovery from inactivation. Measurements were also made of the time course of recovery from inactivation. A depolarizing 100-ms pulse to 0 mV was used to inactivate the sodium current. After such a conditioning depolarization, currents elicited by a 10-ms test pulse slowly increased in amplitude to their preconditioning level. The currents in Fig. 11 *A*, generated by test pulses to −20 mV at 10, 30, 50, and 70 ms after the conditioning depolarization, increased in amplitude with the interval. The rates of recovery of the amplitude of currents generated by test pulses to −20 mV from holding potentials of −80 mV (circles), −100 mV (squares), and −120 mV (diamonds) are illustrated in Fig. 11 *B*. At all three potentials, recovery from inactivation could not be described

by a single exponential. Recovery occurred more rapidly at more negative holding potentials.

Effects of temperature. Consistent effects of changing temperature on the sodium currents were recorded in three cells, whether the temperature was lowered or raised. As the temperature was lowered, the currents became smaller and slower, as illustrated in Fig. 12. The upper traces were recorded at 22°C; the lower traces were recorded immediately after lowering the temperature to 18°C (note the difference in vertical calibrations). The current-voltage curves

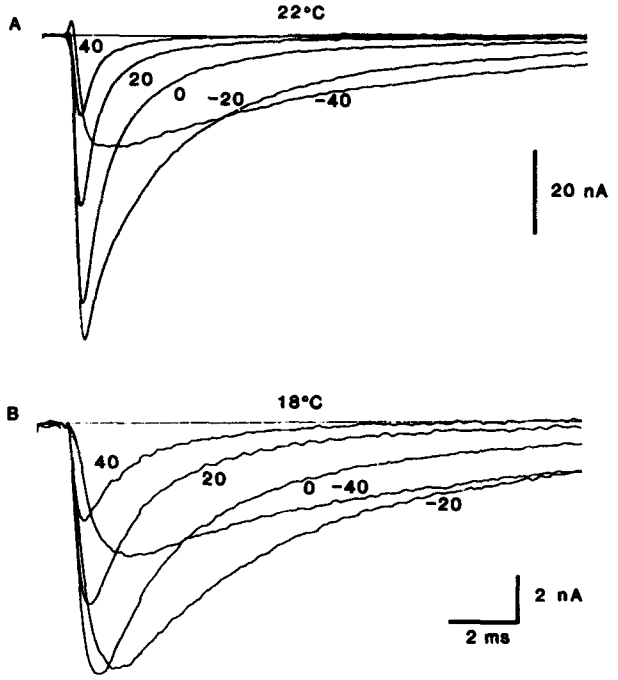

FIGURE 12. Effect of temperature on sodium currents. Sodium currents were generated by pulses from a holding potential of −100 mV to the potentials shown, recorded in one cell at 22°C (*A*) and at 18°C (*B*). Note the difference in the vertical calibrations in *A* and *B*.

recorded in one experiment in which the temperature was raised from 17.5 to 26.5°C (Fig. 13 *A*) show the dependence of current amplitude on temperature. The conductance-voltage curves for two temperatures, 18 and 22°C, in one cell are shown in Fig. 7: it can be seen that the peak conductance fell from 1.16 μS at 22°C to 0.37 μS at 18°C. The k value changed from 7.1 to 13 mV but V' was essentially unchanged. There was a larger fall in current amplitude for the 2.5°C change in temperature between 20°C and 17.5°C than between 22.5°C and 20°C. The maximum current amplitude is plotted semilogarithmically against temperature in Fig. 13 *B*. The line through the points at 20–26.5°C gave a Q_{10}

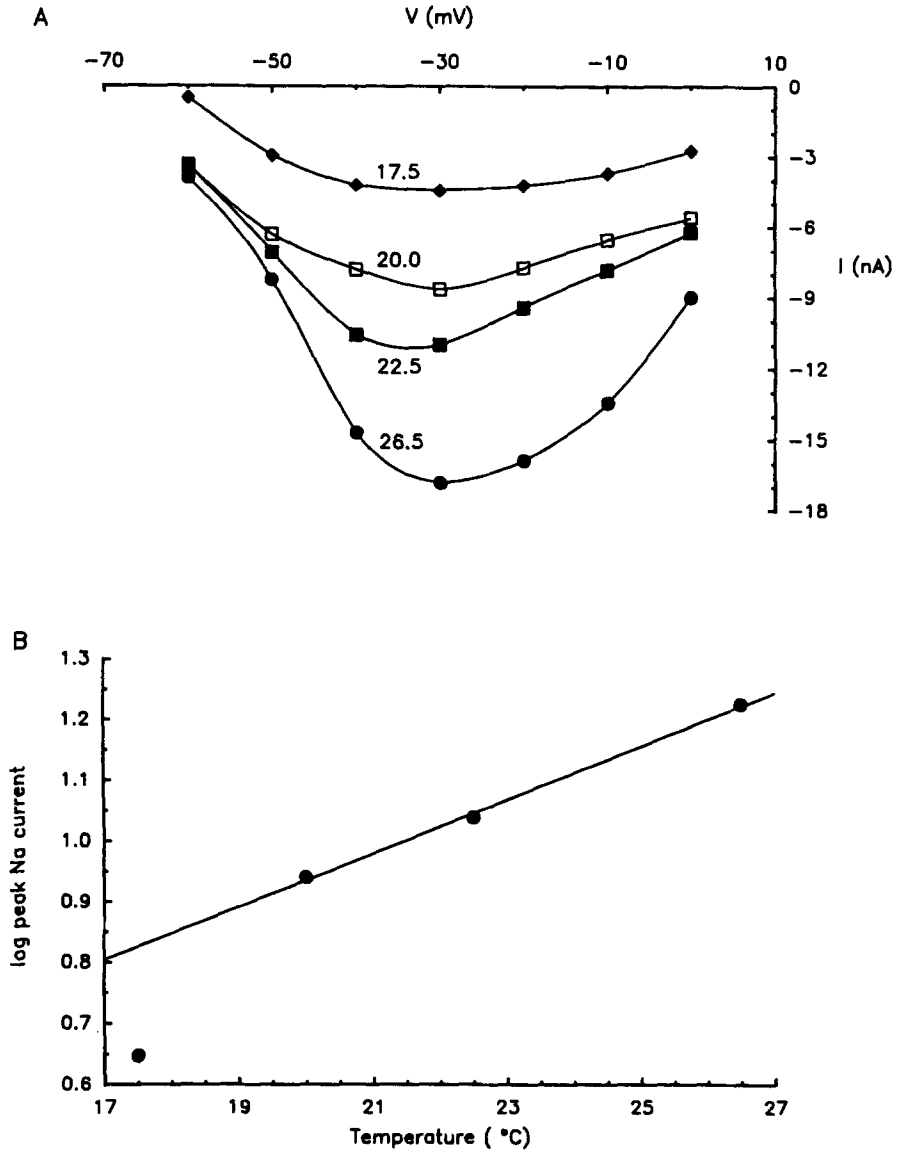

FIGURE 13. Effect of temperature on maximum sodium current. (*A*) Current-voltage curves (peak current) recorded at different temperatures in the same cell. From top: 17.5°C (diamonds); 20°C (open squares); 22.5°C (filled squares); 26.5°C (circles). (*B*) Semilogarithmic plot of maximum sodium current (nanoamperes) (measured at −20 to −40 mV with a holding potential of −100 mV) against temperature (Kelvin). The solid line, drawn by eye through the points from 20 to 27°C, gives a Q_{10} of 1.5.

of 1.5. The current amplitude at 17.5°C is less than expected from the line fitted to the points at the three other temperatures.

A similar phenomenon was seen with time to peak and half-decay times, as

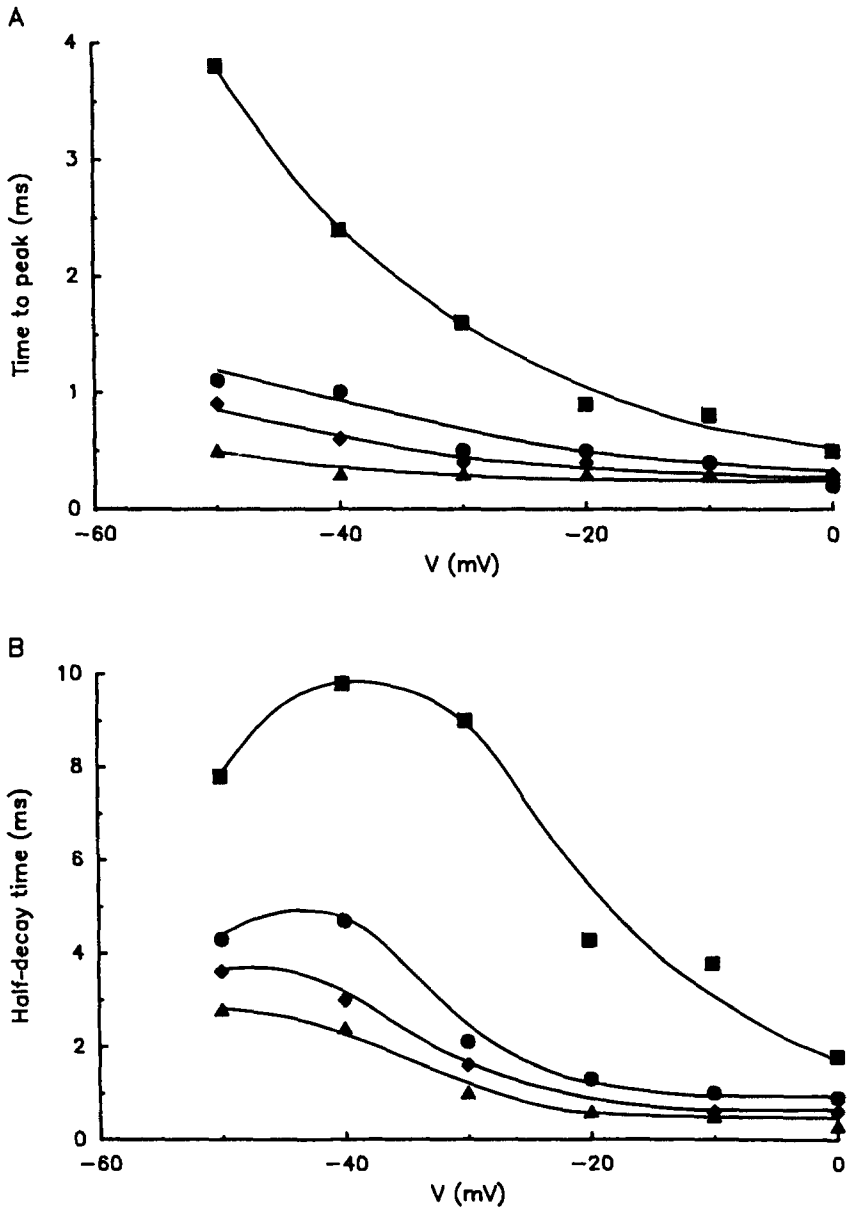

FIGURE 14. Effect of temperature on time course of sodium currents: 17.5°C (squares); 20°C (circles); 22.5°C (diamonds); 26.5°C (triangles). (*A*) Time to peak of sodium currents recorded at different temperatures in the same cell. (*B*) Half-decay times of the same sodium currents at different temperatures.

illustrated in Fig. 14. There appeared to be a steep change in both measures between 17.5 and 20°C. All three cells showed a clear break in the temperature dependence of current amplitude and time course in this temperature range. As

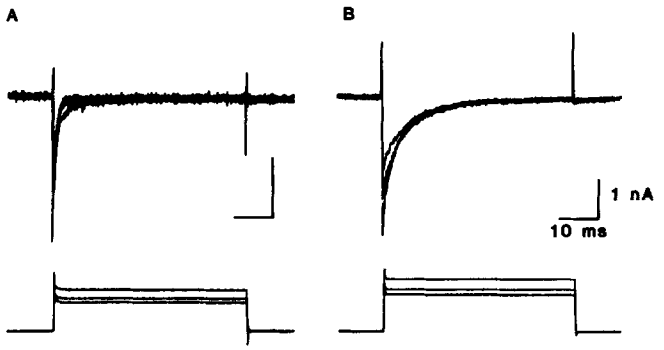

FIGURE 15. Fast sodium currents (*A*) compared with normal sodium currents recorded in a different cell (*B*). The upper traces show sodium currents generated by voltage steps (lower traces) to −35, −30, and −20 mV from a holding potential of −100 mV.

reported for rabbit (Chiu et al., 1979*a*) and rat (Schwarz, 1986) myelinated nerve, it was found that the h_∞ curve shifted to more positive potentials as the temperature was raised.

Sodium Currents with a Faster Time Course

In 15 of the 120 cells studied, the sodium current had a faster time course. This is illustrated in Fig. 15, in which a family of the "fast" sodium currents (*A*) can be compared with sodium currents of the more common type (*B*). The half-decay times measured in three cells with fast currents are given at two potentials in Table I. It is clear that the decay of the fast sodium current is almost an order of magnitude faster than the decay of the slower current. Furthermore, this difference in decay rates is maintained throughout the voltage range examined.

The peak current-voltage relationship for a fast sodium current is shown in Fig. 16*A*. The h_∞ curve is shown in Fig. 16*B* (circles), the line through the points being drawn according to Eq. 3 with V' and k values of −67.6 and 7.4 mV, respectively. These values are similar to those for the slower currents. Peak conductance is plotted against potential in Fig. 16*B* (squares) and the line through the points is drawn according to Eq. 2, with V' and k values of −29 and 5.7 mV, respectively. These curves are very similar to those for the more common sodium currents (see Fig. 10).

TABLE I

Comparison of Time Constants of Decay of Normal and Fast Sodium Currents

V_m	Normal	Fast
mV	*ms*	*ms*
−40	8.8±1.2* (*n* = 9)	0.9 (*n* = 1)
−20	7.4±0.9 (*n* = 9)	0.9±0.2 (*n* = 3)

* Mean ± 1 SD.

DISCUSSION

Dissociated hippocampal neurons were used because they provided the opportunity to characterize depolarization-activated sodium currents in well-clamped

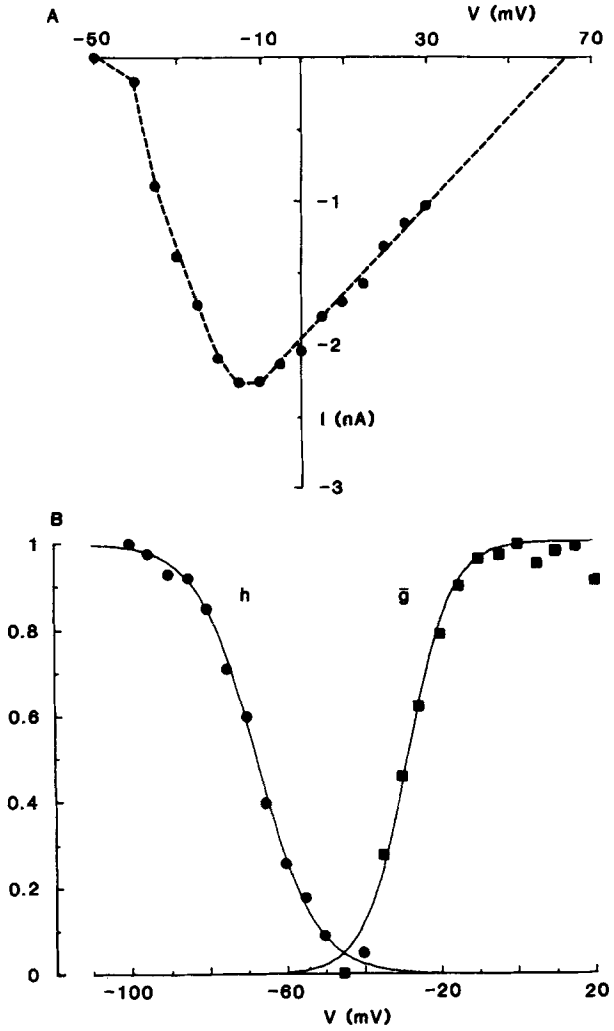

FIGURE 16. Properties of the fast sodium current. (*A*) Current-voltage curve showing the change in amplitude of the sodium current with voltage (holding potential, −100 mV). (*B*) Normalized conductance ($\bar{g}$) (squares) and h (circles), recorded in the same cell, plotted against potential. The solid lines through the data points are the Boltzmann curves of best fit (see Eqs. 2 and 3 in text).

membrane. This is normally not possible in these cells because of the difficulty in controlling potential across areas of membrane in dendrites separated by a significant resistance from a point source of current in the soma (Jack et al.,

1975; Johnston and Brown, 1983). The task becomes even more difficult if there are neurotransmitter-induced shunts across the membrane of the processes. Although the whole-cell patch-clamp technique, combined with a fast, single-electrode clamp, provided voltage control within 500 μs in these cells, it was necessary to work at low temperatures (20–24°C) in order to control potential during the rising phase and peak of some sodium currents. At this temperature, dissociated cells from guinea pig hippocampus, although somewhat depolarized, retained the ability to generate action potentials and proved a suitable preparation for studying the underlying sodium current.

The passive electrical properties of the dissociated hippocampal cells are different in many respects from those measured in CA1 pyramidal cells in situ in brain slices. The depolarized resting potential is probably due, at least in part, to a persistent, nonselective conductance shunt across stumps of broken-off cell processes. If the original resting membrane potential of the cell were −60 mV, a shunt resistance (null potential, 0 mV) equal to twice the input resistance of the cell without such a shunt would reduce the membrane potential to about

TABLE II

Comparison of Passive Properties of Hippocampal CA1 Cells

	V	τ	R_o	R_m	C_m
	mV	*ms*	$10^8\ \Omega$	$k\Omega \cdot cm^2$	$\mu F \cdot cm^{-2}$
Slice*	−65	10–20	0.3–0.6	10	2–4
Dissociated‡	−60	20–36	2–12	—	—
Dissociated	−40	1.2–10	2–10	5.8	1.0
(Corrected)	—	—	(2–16)	(3.6–16)	(10.7)

* Brown et al., 1981; Turner, 1984.

‡ Huguenard and Alger, 1986.

−40 mV. It is also possible that the techniques of cell dissociation and whole-cell clamp, involving internal perfusion of cells with KF or CsF, could have contributed to the depolarization.

The measured input resistance of dissociated cells ranged from 100 to 1,000 MΩ, an order of magnitude greater than in slices (see Table II). Several factors probably contribute to this difference. The dissociation procedure removes the extensive dendritic tree with its synaptic input (Turner and Schwartzkroin, 1980). Furthermore, the presence of fluoride and 10 mM EGTA in the recording electrode would lower the intracellular calcium concentration so that any resting calcium-activated potassium conductance would be reduced. Finally, the leak resistance around an intracellular microelectrode, which can be as low as 20 MΩ (Hodgkin and Nakajima, 1972), would have reduced the input resistance; the whole-cell patch-clamp technique introduces a negligible shunt resistance. On the other hand, the calculated specific membrane resistance of 5.8 ± 1.4 $k\Omega \cdot cm^2$, which takes the loss of membrane area into account, is much lower than the value of 10 $k\Omega \cdot cm^2$ reported for CA1 neurons in slices (Table II). This suggests that the increase in input resistance cannot be attributed to an increase in

specific membrane resistance. Taking both the depolarization and low membrane resistance into account, it seems very likely that there is an electrical leak across the stumps of the fractured processes in these cells. A leak resistance twice the input resistance, as assumed above, would reduce the measured membrane resistance to two-thirds of the true membrane resistance: correcting for such a leak would increase the membrane resistance to $\sim$10 k$\Omega \cdot$cm^2 (Table II). Another possible explanation for the lower membrane resistance in dissociated cells is that, as suggested for motoneurons (Fatt, 1957; Iansek and Redman, 1973), the specific membrane resistance in the soma may be less than in the dendrites.

The time constants of 3–5 ms measured here are lower than the time constants of 10–20 ms reported for CA1 cells in slices (Table II). This difference can probably be attributed to the same factors that caused the low input resistance. The average specific membrane capacity calculated from the input capacitance and membrane area was 1 μF$\cdot$cm^{-2}, close to that expected for cell membranes, which suggests that the calculations of membrane area were reasonably accurate.

It was found to be possible to voltage-clamp the membrane adequately and record ionic currents in these cells. The inward current could be blocked with TTX, it decreased in amplitude when the extracellular concentration of sodium was decreased, and it had a null potential close to the sodium equilibrium potential, typical characteristics of a sodium current. A residual, small, slower, TTX-insensitive inward current, probably a calcium current (Kay et al., 1986), was sometimes seen (Fig. 5 *D*), but it was not examined further. If it had been present, it would have made an insignificant contribution to the total inward current and it was not apparent in many cells (e.g., see Fig. 3). In neurons in slice preparations, calcium currents recorded with electrodes in the soma (Johnston et al., 1980; D. A. Brown and Griffith, 1983) are much larger (1–3 nA) than reported here. Calcium currents have been shown to be very labile (Fenwick et al., 1982; Kostyuk, 1984) and it is possible that the calcium currents in the dissociated cells were "washed out" during the dissociation procedure. Another possibility is that most of the calcium channels may be located on the dendrites (Llinas and Sugimori, 1980; Jahnsen, 1986) and are removed during dissociation. Alternatively, it is possible that the TTX-insensitive inward current was a sodium current similar to the TTX-insensitive sodium current seen in nodose ganglion cells (Ikeda et al., 1986); further experiments will be needed to define its nature.

A slow, noninactivating, TTX-sensitive sodium current found in rat hippocampal CA1 neurons by French and Gage (1985) (see also Stafstrom et al., 1985) could also be seen in dissociated neurons. This current, like the calcium current, was relatively very small (the maximum amplitude was always $<$0.6 nA) and had little effect on the amplitude or time course of the larger sodium current.

The sodium currents in most of the cells were slower than reported for some other mammalian cells at the same temperature (Chiu et al., 1979*a*, *b*; Kostyuk et al., 1981; Neumcke and Stampfli, 1982; Fenwick et al., 1982; Matteson and Armstrong, 1984; Dubinsky and Oxford, 1984; Vandenberg and Horn, 1984; Belluzzi and Sacchi, 1986; Carbone and Lux, 1986). If single channels had a

conductance of 18 pS (Sigworth and Neher, 1980; Stühmer et al., 1987), the maximum sodium conductance of 7.2–14.7 $mS \cdot cm^{-2}$ corresponds to 5–10 sodium channels per μm^2. This is similar to the sodium channel density on bovine chromaffin cells (Fenwick et al., 1982) but about five times the density in GH_3 cells (Matteson and Armstrong, 1984; Dubinsky and Oxford, 1984). By comparison, there are 200–300 sodium channels per μm^2 in neuroblastoma cells (Moolenaar and Spector, 1979), in frog and rat node of Ranvier, and in squid giant axon (see Hille, 1984, for review). Using a membrane capacitance of 1 $\mu F \cdot cm^{-2}$, a sodium channel density of 5–10 channels per μm^2, a sodium equilibrium potential of 70 mV, and a peak current of −20 mV, the rate of rise of an action potential would be 600–1,200 $V \cdot s^{-1}$. This is close to the measured rate of rise of action potentials of 600–1,000 $V \cdot s^{-1}$ and indicates that the sodium current described here is responsible for the rising phase of the action potentials recorded in these cells.

Both activation and inactivation of sodium channels occurred at more negative potentials (Fig. 9) than found in other mammalian neurons (Barrett and Crill, 1980; Fenwick et al., 1982; Matteson and Armstrong, 1984; Fernandez et al., 1984; Vandenberg and Horn, 1984). However, activation of mammalian brain sodium channels expressed in oocytes (Stühmer et al., 1987) occurred at potentials similar to those seen here. Some of the differences in the voltage dependence of activation and particularly inactivation may be associated with differences in temperature (Schwarz, 1986; this article). A further difference might be the introduction of fluoride ions into the cell interior. It has been suggested (Fernandez et al., 1984) that sodium channel activation and inactivation curves slowly shift to more negative potentials when the intracellular solution contains fluoride ions, but this does not seem to happen in squid axon (Adams and Oxford, 1983). The records from most cells in this study were taken at least 10–15 min after obtaining access to the interior of the cell. Although we did not systematically look for a change in voltage dependence with time, no changes in voltage dependence of activation or inactivation were seen during an experiment.

In many preparations, particularly at the node of Ranvier of both frog and rat nerve (Chiu, 1977; Neumcke and Stampfli, 1982) and rat heart (A. M. Brown et al., 1981), sodium current decay follows a biexponential time course. In hippocampal cells, however, only one time constant was generally observed, although in several cells and particularly at depolarized potentials, two time constants were evident (Fig. 9). Thus, inactivation in hippocampal cells is more similar to that seen in GH_3 cells (Vandenberg and Horn, 1984) than in rat node of Ranvier (Neumcke and Stampfli, 1982; Schwarz, 1986).

Despite the variety of cell morphologies obtained after dissociation, the sodium conductance of most cells had very similar properties. A few cells had much more rapid sodium currents (Fig. 13). It has been suggested that injection of mRNA isolated from rat brain into *Xenopus* oocytes yields two populations of sodium channels with different open times (Gundersen et al., 1983). In addition, there are at least two different kinds of sodium channel–specific mRNA in rat brain (Noda et al., 1986). These observations may explain the two different types

of channel kinetics observed in the dissociated cells. Action potentials in interneurons in the hippocampus and cortex have a faster time course than normal and do not accommodate (Schwartzkroin and Mathers, 1978; McCormick et al., 1985). It is possible that the underlying sodium channels also have faster kinetics. Fast sodium currents can also be recorded from glial cells (Bevan et al., 1985; Gibb, A. J., unpublished observations). The dissociated cells with faster sodium currents may have been interneurons or glial cells.

We thank F. Dreyer, A. Dulhunty, G. Lamb, D. McKinnon, and S. Redman for helpful comments, R. Taylor for assistance with software, and R. Malbon and A. Andrews for technical assistance.

Original version received 30 March 1987 and accepted version received 11 September 1987.

REFERENCES

Adams, D. J., and G. S. Oxford. 1983. Interaction of internal anions with potassium channels of the squid giant axon. *Journal of General Physiology.* 82:429–448.

Adrian, R. H., W. K. Chandler, and A. L. Hodgkin. 1970. Slow changes in potassium permeability in skeletal muscle. *Journal of Physiology.* 208:645–688.

Barrett, J. N., and W. E. Crill. 1980. Voltage clamp of cat motoneurone somata: properties of the fast inward current. *Journal of Physiology.* 304:231–249.

Belluzzi, O., and O. Sacchi. 1986. A quantitative description of the sodium current in the rat sympathetic neurone. *Journal of Physiology.* 380:275–291.

Bevan, S., S. Y. Chiu, P. T. A. Gray, and J. M. Ritchie. 1985. The presence of voltage gated sodium potassium and chloride channels in rat cultured astrocytes. *Proceedings of the Royal Society of London, Series B.* 225:299–313.

Brenneke, R., and B. Lindermann. 1974. Theory of membrane voltage clamp with discontinuous feedback through a pulsed current clamp. *Review of Scientific Instrumentation.* 45:184–188.

Brown, A. M., K. S. Lee, and T. Powell. 1981. Sodium current in single rat heart muscle cells. *Journal of Physiology.* 318:479–500.

Brown, D. A., and W. H. Griffith. 1983. Persistent slow inward calcium current in voltage clamped hippocampal neurons of the guinea pig. *Journal of Physiology.* 337:303–320.

Brown, T. H., R. A. Fricke, and D. H. Perkel. 1981. Passive electrical constants in three classes of hippocampal neurons. *Journal of Neurophysiology.* 46:812–827.

Carbone, E., and H. D. Lux. 1986. Sodium currents in cultured chick dorsal root ganglion neurones. *European Biophysics Journal.* 13:259–271.

Chiu, S. Y. 1977. Inactivation of sodium channels: second order kinetics in myelinated nerve. *Journal of Physiology.* 273:573–596.

Chiu, S. Y., H. E. Mrose, and J. M. Ritchie. 1979*a*. Anomalous temperature dependence of the sodium conductance in rabbit nerve compared with frog nerve. *Nature.* 279:327–328.

Chiu, S. Y., J. M. Ritchie, R. B. Rogart, and D. Stagg. 1979*b*. A quantitative description of membrane currents in rabbit myelinated nerve fibres. *Journal of Physiology.* 292:149–166.

Dubinsky, J. M., and G. S. Oxford. 1984. Ionic currents in two strains of rat anterior pituitary tumor cells. *Journal of General Physiology.* 83:309–339.

Fatt, P. 1957. Sequence of events in synaptic activation of a motoneurone. *Journal of Neurophysiology.* 20:61–80.

Fenwick, E. M., A. Marty, and E. Neher. 1982. Sodium and calcium channels in bovine chromaffin cells. *Journal of Physiology.* 331:599–635.

Fernandez, J., A. P. Fox, and S. Krasne. 1984. Membrane patches and whole-cell membranes: a comparison of electrical properties in rat clonal pituitary (GH3) cells. *Journal of Physiology.* 356:564–585.

Finkel, A. S., and S. Redman. 1985. Theory and operation of a single microelectrode voltage clamp. *Journal of Neuroscience Methods.* 11:101–127.

French, C. R., and P. W. Gage. 1985. A threshold sodium current in pyramidal cells in rat hippocampus. *Neuroscience Letters.* 56:289–293.

Gray, J., and D. Johnston. 1985. Rectification of single GABA-gated chloride currents in adult hippocampal neurones. *Journal of Neurophysiology.* 54:134–142.

Gundersen, C. B., R. Miledi, and I. Parker. 1983. Voltage operated channels induced by foreign messenger RNA in *Xenopus* oocytes. *Proceedings of the Royal Society of London, Series B.* 220:131–140.

Hamill, O. P., A. Marty, E. Neher, B. Sakmann, and F. Sigworth. 1981. Improved patch clamp techniques for high-resolution current recordings from cells and cell-free membrane patches. *Pflügers Archiv.* 391:85–100.

Hille, B. 1984. Ionic Channels of Excitable Membranes. Sinauer Associates, Inc., Sunderland, MA. 426 pp.

Hodgkin, A. L., and A. F. Huxley. 1952*a*. The components of membrane conductance in the giant axon of *Loligo*. *Journal of Physiology.* 116:473–496.

Hodgkin, A. L., and A. F. Huxley. 1952*b*. The dual effect of membrane potential on sodium conductance in the giant axon of *Loligo*. *Journal of Physiology.* 116:497–506.

Hodgkin, A. L., and S. Nakajima. 1972. The effect of diameter on the electrical constants of frog skeletal muscle fibres. *Journal of Physiology.* 221:105–120.

Huguenard, J. R., and B. E. Alger. 1986. Whole cell voltage clamp study of the fading of GABA-activated currents in acutely dissociated hippocampal neurons. *Journal of Neurophysiology.* 56:1–17.

Iansek, R., and S. J. Redman. 1973. An analysis of the cable properties of spinal motoneurones using a brief intracellular current pulse. *Journal of Physiology.* 243:613–636.

Ikeda, S. R., G. G. Schofield, and F. F. Weight. 1986. Na^+ and Ca^{2+} currents of acutely isolated adult rat nodose ganglion cells. *Journal of Neurophysiology.* 53:527–539.

Jack, J. J. B., D. Noble, and R. W. Tsien. 1975. Electric Current Flow in Excitable Cells. Clarendon Press, Oxford. 502 pp.

Jahnsen, H. 1986. Extracellular activation and membrane conductances of neurones in the guinea pig deep cerebellar nuclei *in vitro*. *Journal of Physiology.* 372:149–168.

Johnston, C., and T. H. Brown. 1983. Interpretation of voltage clamp measurement in hippocampal neurones. *Journal of Neurophysiology.* 50:464–486.

Johnston, D., J. L. Hablitz, and W. A. Wilson. 1980. Voltage clamp discloses slow inward current in hippocampal burst-firing neurones. *Nature.* 286:391–393.

Kay, A. R., R. Miles, and R. K. S. Wong. 1986. Intracellular fluoride alters the kinetic properties of calcium currents facilitating the investigation of synaptic events in hippocampal neurons. *Journal of Neuroscience.* 6:2915–2920.

Kay, A. R., and R. K. S. Wong. 1986. Isolation of neurones suitable for patch-clamping from adult mammalian central nervous systems. *Journal of Neuroscience Methods.* 16:227–238.

Kostyuk, P. G. 1984. Intracellular perfusion of nerve cells and its effects on membrane currents. *Physiological Reviews.* 64:435–454.

Kostyuk, P. G., N. S. Veselosky, and A. Y. Tsyndrenko. 1981. Ionic currents in the somatic membrane of rat dorsal root ganglion: sodium currents. *Neuroscience.* 6:2423–2430.

Llinas, R., and M. Sugimori. 1980. Electrophysiological properties of in vitro Purkinje cell somata in mammalian cerebellar slices. *Journal of Physiology.* 305:171–195.

Matteson, D. R., and C. M. Armstrong. 1984. Na and Ca channels in a transformed line of anterior pituitary cells. *Journal of General Physiology.* 83:371–394.

McCormick, D. A., B. W. Connors, J. Lighthall, and D. A. Prince. 1985. Comparative electrophysiology of pyramidal and sparsely spiny stellate neurons of the neocortex. *Journal of Neurophysiology.* 54:782–806.

Moolenaar, W. H., and I. Spector. 1978. Ionic currents in cultured mouse neuroblastoma cells under voltage clamp conditions. *Journal of Physiology.* 278:265–286.

Neumcke, B., and R. Stampfli. 1982. Sodium currents and sodium current fluctuations in rat myelinated nerve fibres. *Journal of Physiology.* 329:163–184.

Noda, M., T. Ikeda, T. Kayano, H. Suzuki, H. Takeshima, M. Kurasaki, H. Takahashi, and S. Numa. 1986. Existence of distinct sodium channel messenger RNA's in rat brain. *Nature.* 320:188–192.

Numann, R. E., and R. K. S. Wong. 1984. Voltage-clamp study of GABA response desensitization in single pyramidal cells dissociated from the hippocampus of adult guinea pigs. *Neuroscience Letters.* 47:289–295.

Rall, W. 1977. Core conductor theory and cable properties of neurons. *In* Handbook of Physiology. The Nervous System. American Physiological Society, Bethesda, MD. 39–97.

Sah, P., A. J. Gibb, and P. W. Gage. 1986. Ionic currents in acutely dissociated adult hippocampal neurones. *Neuroscience Letters.* 23(Suppl.):77.

Schwartzkroin, P. A., and L. H. Mathers. 1978. Physiological and morphological identification of a nonpyramidal hippocampal cell type. *Brain Research.* 157:1–10.

Schwarz, J. R. 1986. The effect of temperature on Na currents in rat myelinated nerve fibres. *Pflügers Archiv.* 406:397–404.

Sigworth, F. J., and E. Neher. 1980. Single Na^+ channel currents observed in cultured rat muscle cells. *Nature.* 287:447–449.

Stafstrom, C. E., P. C. Schwindt, M. C. Chubb, and W. E. Crill. 1985. Repetitive firing in layer V neurons from cat neocortex in vitro. *Journal of Neurophysiology.* 52:264–277.

Stühmer, W., C. Methfessel, B. Sakmann, M. Noda, and S. Numa. 1987. Patch clamp characterization of sodium channels expressed from rat brain cDNA. *European Biophysics Journal.* 14:131–138.

Turner, D. A. 1984. Segmental cable evaluation of somatic transients in hippocampal neurons (CA1, CA3 and dentate). *Biophysical Journal.* 46:73–84.

Turner, D. A., and P. A. Schwartzkroin. 1980. Steady-state electronic analysis of intracellularly-stained hippocampal neurons. *Journal of Neurophysiology.* 44:184–199.

Vandenberg, C. A., and R. Horn. 1984. Inactivation viewed through single sodium channels. *Journal of General Physiology.* 84:535–564.